M.V. USHCATS

Admiral Makarov National University of Shipbuilding
(9, Prosp. Stalingrad Heroes, Mykolaiv 54025, Ukraine; e-mail: mykhailo.ushcats@nuos.edu.ua)

PACS 05.20.-y, 05.70.Fh, 64.70.F-, 64.60.-i

VIRIAL COEFFICIENTS OF MODIFIED LENNARD-JONES POTENTIAL

A modified Lennard-Jones potential with a finite interaction radius, which maintains the realistic behavior of its parent and greatly simplifies the numerical simulation of high-density thermodynamic systems, has been considered. The virial coefficients of this potential have been calculated up to the fifth order, inclusive, in a wide range of temperatures. The modified potential can be applied not only in numerical experiments but also in theoretical studies. It is proposed as a reference model to test the adequacy of various theoretical and experimental approaches.

K e y w o r d s: virial coefficient, irreducible cluster integral, Mayer function, spinodal, binodal.

1. Introduction

While studying the behavior of thermodynamic systems with high densities, the actual interaction between molecules is most often approximated by certain simplified analytical expressions for the force or the potential energy (the potential) of interaction for every molecular pair [1]. One of the most known and widely used model potentials of this kind is the two-parameter 12–6 Lennard-Jones (LJ) potential [2,3], in which the repulsion energy is reciprocal to the 12-th power of the intermolecular distance, and the attraction one to the 6-th power,

$$u_{\mathrm{LJ}}(r) = 4\epsilon\left[\left(\frac{\sigma}{r}\right)^{12} - \left(\frac{\sigma}{r}\right)^{6}\right], \qquad (1)$$

where ϵ is the bond dissociation energy for the pair, and σ a characteristic distance, at which the potential equals zero (Fig. 1). This potential is used to describe various aggregate states of simple substances, such as, e.g., inert gases [4, 5].

Unfortunately, the infinite radius of interaction in the LJ potential (1) creates considerable technical difficulties when carrying out numerical experiments both on the basis of the Monte Carlo method [4–11] and the method of molecular dynamics (MD) [9–14]. In practice, since the potential quickly tends to zero as the distance grows, it is usually "truncated" at a definite distance. In other words, it is neglected at larger distances.

However, the application of such a "truncated" Lennard-Jones (LJT) potential brings us to other difficulties: the potential is discontinuous at the "truncation" distance, so that the interaction force becomes infinitely large here, which is inadmissible, especially at MD simulations. This problem, in its turn, is resolved by shifting the potential upwards by a constant value, which is equal to the absolute potential value at the "truncation" distance, and the final potential has no break (nevertheless, the break in the force still remains at that). Just this "truncated and shifted" Lennard-Jones (LJTS) potential rather than the "primordial" LJ one (Eq. (1)) was used in the majority of numerical experiments [6–14].

In time, the rejection of weak attraction at large distances was found to bring about an appreciable difference between the results of simulations. For instance, the critical temperatures for the LJT and LJTS potentials with a typical truncation radius value of 2.5σ were found to be by approximately 20%

lower in comparison with that for the LJ potential (1) [9, 14–16]. Certainly, there exist the techniques that approximately take the rejected part of the potential into account and correspondingly rescale the results obtained [9, 14]. However, the unavoidable errors arising in this case complicate the comparison of the data obtained in various experimental and theoretical researches.

In recent years, the so-called modified Lennard-Jones (mLJ) potential becomes more and more popular in computer experiments [17–19]. It looks like

$$u(r) = \begin{cases} 4\epsilon\left[\left(\frac{\sigma}{r}\right)^{12} - \left(\frac{\sigma}{r}\right)^{6}\right] + c_1; & r \le 2.3\sigma, \\ c_2\left(\frac{\sigma}{r}\right)^{12} + c_3\left(\frac{\sigma}{r}\right)^{6} + c_4\left(\frac{r}{\sigma}\right)^{2} + c_5; & 2.3\sigma < r < 2.5\sigma, \\ 0; & r \ge 2.5\sigma. \end{cases} \quad (2)$$

where $c_1 = 0.0163169237\epsilon$, $c_2 = 3136.5686\epsilon$, $c_3 = -68.069\epsilon$, $c_4 = -0.0833111261\epsilon$, and $c_5 = 0.746882273\epsilon$.

This potential, as well as its derivative (the corresponding interaction force) has no breaks and vanishes at the distance 2.5σ (Fig. 1). Those properties distinguish the mLJ potential among the others (LJ, LJT, and LJTS) and make it an admissible candidate for the role of universal standard while comparing various theoretical and experimental approaches and estimating their adequacy.

On the other hand, the mLJ potential has not found a wide application in theoretical researches till now. In particular, the virial coefficients up to the eighth order are known for the LJ potential [20, 21], and up to the fifth order for the LJTS one [16]. At the same time, the data concerning the coefficients for the mLJ potential are absent for today. Therefore, this work aimed at calculating the virial coefficients for the modified Lennard-Jones potential (2) up to the fifth order and in a wide temperature interval, which could be used in theoretical researches and for the comparison with available experimental data.

2. Calculation Technique

According to book [22], the virial coefficient of the $(k+1)$-th order in the power series expansion of the pressure in the density parameter

$$B_{k+1} = -\frac{k}{k+1}\beta_k, \quad (3)$$

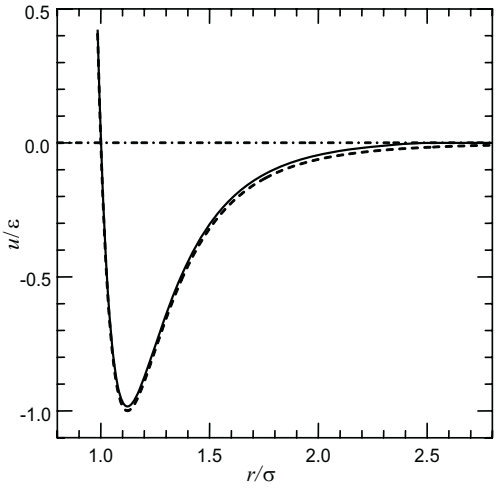

Fig. 1. 12-6 Lennard-Jones potential (dashed curve) and a modified Lennard-Jones potential (solid curve)

where β_k is the so-called irreducible cluster integral of the k-th order. The latter is defined as follows. For an arbitrary pair of molecules with a given interaction potential, let us introduce the Mayer function

$$f(r) = \exp\left(-\frac{u(r)}{kT}\right) - 1.$$

Then, β_k is defined as the integral of the sum of all possible products of Mayer functions for $(k+1)$ molecules over their configuration phase space divided by $k!V$, that cannot be expressed in terms of low-order irreducible integrals.

Figure 2 demonstrates all graphs corresponding to the irreducible integrals of the first (a), second (b), third (c), and fourth (d) orders. Every Mayer function is conditionally represented by a line connecting two molecules. The multiplicity of each diagram, which takes into account all possible permutations of molecular indices, is also indicated.

Integration over the configurational space of one of the molecules (conditionally, let it be molecule 1) gives the multiplier V, the system volume, which is cancelled out with the volume parameter in the denominator. So we obtain only integration over the relative positions of other molecules (in practice, since the Mayer function decreases rapidly as the distance grows, the integration is performed within infinite limits).

Graphs with $k > 2$ can be grouped together (Fig. 3). Integrals within every group differ from

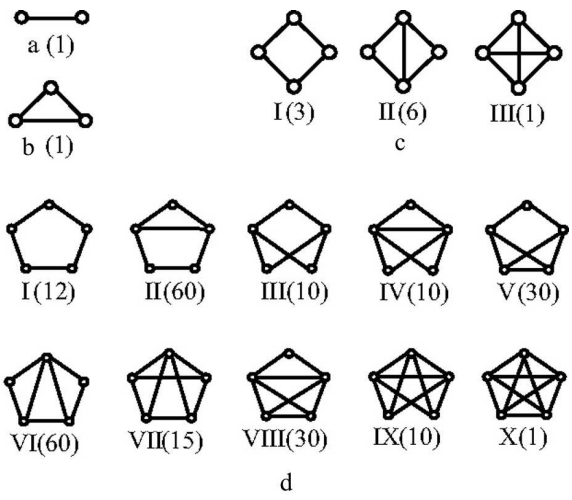

Fig. 2. Irreducible graphs: two- (a), three- (b), four- (c), and five-particle (d) ones. The graph multiplicities are indicated in the parentheses

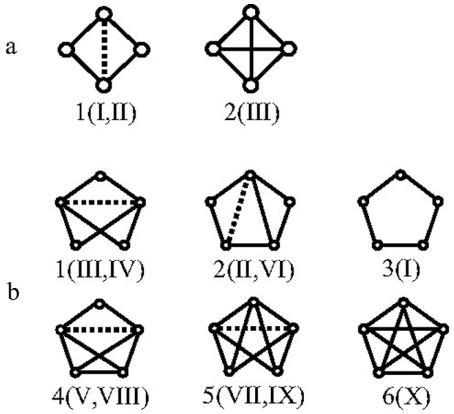

Fig. 3. Groups of similar graphs for the third (a) and fourth (b) irreducible integrals. The numbers of corresponding graphs in Fig. 2 are indicated in the parentheses

one another by the presence or absence of one Mayer function (dotted lines in Fig. 3), and only the second group of four-particle integrals (a) and the third and sixth groups of five-particle ones (b) contain a single graph that differs substantially from the others.

Instead of the distance between particles r_{ij}, let us introduce the dimensionless square of this quantity, $s_{ij} = r_{ij}^2/\sigma^2$, and the function $F(s) = f(\sigma\sqrt{s})$ instead of the corresponding Mayer function. Such a change of variables unifies the integration process and makes it considerably simpler. First, the dependence on the integration variable becomes weaker, which is favorable for the calculation accuracy. In addition, the irreducible integrals (their dimensionality is equal to the volume raised to the power k) can be defined in the dimensionless form, $\beta'_k = -\beta_k/\sigma^{3k}$. The simplest one is the first irreducible integral

$$\beta'_1 = 2\pi \int_0^\infty F(s)\sqrt{s}ds. \tag{4}$$

The corresponding second virial coefficient is $B_2 = \beta_1/2$.

In each many-particle (with $k > 1$) irreducible integral, we can select three molecules (i, j, and n), for which particle n is "connected" by means of the Mayer functions with two other "basic" particles (i and j), with the latter, in turn, can be either "connected" with each other or not, depending on the specific diagram. If particle n, in addition to its connections with particles i and j, is not connected with any other, the integral over all its possible positions, provided that the positions of particles i and j are fixed, looks like

$$\frac{\pi\sigma^3}{2\sqrt{s_{ij}}} \int_0^\infty F(s_{in})\, ds_{in} \int_{\left(\sqrt{s_{ij}}-\sqrt{s_{in}}\right)^2}^{\left(\sqrt{s_{ij}}+\sqrt{s_{in}}\right)^2} F(s_{jn})\, ds_{jn}.$$

Let us introduce the function

$$\Phi(s) = \int_0^\infty F(s_1)\, ds_1 \int_{\left(\sqrt{s}-\sqrt{s_1}\right)^2}^{\left(\sqrt{s}+\sqrt{s_1}\right)^2} F(s_2)\, ds_2. \tag{5}$$

Then, the dimensionless expression for the second irreducible integral reads (we use the notation $s = s_{12}$)

$$\beta'_2 = \frac{\pi^2}{2} \int_0^\infty F(s)\Phi(s)\, ds. \tag{6}$$

Integrals corresponding to the first graph group for the third irreducible integral (Fig. 3, a) and to the first graph group for the fourth irreducible integral (Fig. 3, b) are expressed analogously:

$$\beta'_{31} = \frac{1}{3!}\frac{\pi^3}{2} \int_0^\infty [3 + 6F(s)]\, \Phi^2(s)\, \frac{ds}{\sqrt{s}}, \tag{7}$$

and

$$\beta'_{41} = \frac{10}{4!}\frac{\pi^4}{4}\int\limits_0^\infty [1+F(s)]\,\Phi^3(s)\,\frac{ds}{s}, \tag{8}$$

respectively. The same function (5) can be used to express more cumbersome formulas for the integrals of the second and third graph groups for the fourth irreducible integral (Fig. 3, b):

$$\begin{aligned}
\beta'_{42} &= \frac{60}{4!}\frac{\pi^4}{4}\int\limits_0^\infty [1+F(s)]\,\Phi(s)\,\frac{ds}{\sqrt{s}}\times \\
&\times \int\limits_0^\infty F(s_1)\,\Phi(s_1)\,\frac{ds_1}{\sqrt{s_1}} \int\limits_{\left(\sqrt{s}-\sqrt{s_1}\right)^2}^{\left(\sqrt{s}+\sqrt{s_1}\right)^2} F(s_2)\,ds_2; \\
\beta'_{43} &= \frac{12}{4!}\frac{\pi^4}{4}\int\limits_0^\infty \Phi(s)\,\frac{ds}{\sqrt{s}}\int\limits_0^\infty \Phi(s_1)\,\frac{ds_1}{\sqrt{s_1}}\times \\
&\times \int\limits_{\left(\sqrt{s}-\sqrt{s_1}\right)^2}^{\left(\sqrt{s}+\sqrt{s_1}\right)^2} F(s_2)\,ds_2.
\end{aligned} \tag{9}$$

In the cases where particle n from the group of three molecules ijn and particle m from the group ijm are "connected", we introduce one more function

$$\begin{aligned}
\Psi(s_{ij}, s_{in}, s_{jn}) &= \int\limits_0^\infty F(s_{im})\,ds_{im}\times \\
&\times \int\limits_{\left(\sqrt{s_{im}}-\sqrt{s_{ij}}\right)^2}^{\left(\sqrt{s_{im}}+\sqrt{s_{ij}}\right)^2} F(s_{jm})\,ds_{jm}\int\limits_0^\pi F(s_{nm})\,d\varphi,
\end{aligned} \tag{10}$$

where $s_{nm}(s_{ij}, s_{in}, s_{jn}, s_{im}, s_{jm}, \varphi)$ is the dimensionless squared distance between particles n and m, and φ is the angle between planes ijn and ijm. Then, integrals corresponding to graph 2 for the third irreducible integral (Fig. 3,a) and the groups of graphs 4 and 5 for the fourth irreducible integral (Fig. 3,b) are expressed as follows:

$$\begin{aligned}
\beta'_{32} &= \frac{1}{3!}\frac{\pi^2}{2}\int\limits_0^\infty F(s)\,\frac{ds}{\sqrt{s}}\int\limits_0^\infty F(s_1)\,ds_1\times \\
&\times \int\limits_{\left(\sqrt{s}-\sqrt{s_1}\right)^2}^{\left(\sqrt{s}+\sqrt{s_1}\right)^2} F(s_2)\,ds_2\Psi(s, s_1, s_2);
\end{aligned}$$

$$\begin{aligned}
\beta'_{44} &= \frac{30}{4!}\frac{\pi^3}{4}\int\limits_0^\infty [1+F(s)]\,\frac{\Phi(s)\,ds}{s}\int\limits_0^\infty F(s_1)\,ds_1\times \\
&\times \int\limits_{\left(\sqrt{s}-\sqrt{s_1}\right)^2}^{\left(\sqrt{s}+\sqrt{s_1}\right)^2} F(s_2)\,ds_2\Psi(s, s_1, s_2); \\
\beta'_{45} &= \frac{1}{4!}\frac{\pi^2}{4}\int\limits_0^\infty [15+10F(s)]\,\frac{ds}{s}\int\limits_0^\infty F(s_1)\,ds_1\times \\
&\times \int\limits_{\left(\sqrt{s}-\sqrt{s_1}\right)^2}^{\left(\sqrt{s}+\sqrt{s_1}\right)^2} F(s_2)\,ds_2\Psi^2(s, s_1, s_2).
\end{aligned} \tag{11}$$

The most complicated is the expression for the integral that corresponds to the last (with ten connections) graph (graph 6) in Fig. 3,b:

$$\begin{aligned}
\beta'_{46} &= \frac{1}{4!}\frac{\pi^2}{8}\int\limits_0^\infty F(s)\,\frac{ds}{s}\int\limits_\infty dS_3\int\limits_\infty dS_4\int\limits_\infty dS_5\times \\
&\times \int\limits_0^\pi F(s_{34})\,d\varphi_{34}\int\limits_0^{2\pi} F(s_{45})\,F(s_{35})\,d\varphi_{35},
\end{aligned} \tag{12}$$

where

$$\int\limits_\infty dS_i f = \int\limits_0^\infty F(s_{1i})\,ds_{1i}\int\limits_{\left(\sqrt{s_{1i}}-\sqrt{s}\right)^2}^{\left(\sqrt{s_{1i}}+\sqrt{s}\right)^2} F(s_{2i})\,ds_{2i}f,$$

φ_{34} is the angle between planes 123 and 124, and φ_{35} between planes 123 and 125.

3. Results

The numerical integration in Eqs. (4), (6)–(9), (11), and (12) was carried out with the use of the Gauss method, which optimally combines accuracy and simplicity [23]. With that end in view, the tables of integration nodes and weights were preliminarily created for various node numbers n = 7, 10, 15, 20, 25, 30, 40, 60, 80, 100, and 120.

The calculation of the first irreducible integral in Eq. (4) to an arbitrary given accuracy does not cause any technical difficulties. Function (5) includes a double integral, but its preliminary tabulation at the integration nodes makes the calculation of integrals β'_2, β'_{31}, and β'_{41} in Eqs. (6)–(8) as simple as that of β'_1.

The trivariate integration in Eq. (9) with the use of the same tabulated function makes the calculation of β'_{42} and β'_{43} somewhat complicated. However,

Virial coefficients of the modified Lennard-Jones potential (2) for various dimensionless temperatures (the calculation accuracy corresponds to the last significant digit)

T^*	B'_2	B'_3	B'_4	B'_5	T^*	B'_2	B'_3	B'_4	B'_5
0.2	−208.38	-5.509×10^5	-1.230×10^{10}	-9.0×10^{14}	1.2	−2.9095	2.9315	3.629	−0.763
0.3	−51.861	−7096	-4.689×10^6	-5.77×10^9	1.3	−2.4600	2.7670	2.682	−2.41
0.4	−25.141	−671.2	-8.981×10^4	-1.81×10^7	1.4	−2.0897	2.5913	1.997	−2.74
0.5	−15.583	−128.4	−6672	-4.62×10^5	1.5	−1.7797	2.4271	1.537	−2.45
0.6	−10.881	−32.12	−901.5	-2.98×10^4	1.7	−1.2904	2.1555	1.061	−1.37
0.7	−8.1321	−7.704	−156.54	-2.99×10^3	2.0	−0.77162	1.8788	0.8810	-3.63×10^{-2}
0.75	−7.1514	−2.960	−65.40	-1.01×10^3	2.5	−0.22426	1.6324	0.9690	1.00
0.8	−6.3433	−0.2625	−25.128	−341	3.0	0.11540	1.5149	1.0978	1.318
0.85	−5.6667	1.2842	−7.107	−107	4.0	0.50756	1.4159	1.2330	1.354
0.9	−5.0924	2.1648	0.8040	−25.9	5.0	0.72157	1.3731	1.2590	1.229
0.95	−4.5991	2.6511	4.022	−0.481	7.0	0.93849	1.32076	1.2007	0.9840
1.0	−4.1711	2.9005	5.053	5.43	10.0	1.07058	1.25563	1.0686	0.7421
1.05	−3.7964	3.0065	5.090	4.95	15.0	1.13951	1.16069	0.88970	0.5219
1.1	−3.4658	3.0260	4.705	2.86	20.0	1.15292	1.08246	0.76472	0.4012

this difficulty does not affect practically the rate of calculations in modern computers (even the general-purpose personal ones).

A basically different situation arises at the six-fold integration in Eq. (11) and, the more so, at the nine-fold one in Eq. (12). In particular, the procedure of calculation of the parameter β'_{32} or the sum $\beta'_{44}+\beta'_{45}$ with the integration node number $n = 30$ required about 1.5 min on a PC with the central processor Intel Core i5 2.67 GHz, whereas the corresponding calculations of a single β'_{46}-value would require about a month.

However, the modern graphic processors can implement the multithreading at a hard-ware level, which makes repeated simple operations with float numbers hundreds times more efficient in comparison with analogous calculations on the basis of a central processor. An opportunity to apply the computing functions of a graphic processor is provided for today by the CUDA platform and the DirectX 11 Compute Shader technology in approximately equal scopes. Therefore, the six-fold integration in Eq. (11) and the nine-fold one in Eq. (12) were adapted to multithreaded calculations. In the case of integrals (11), a two-dimensional $s_1 \times s_2$ mesh of nodes was created for every node s, and the function $\Psi(s, s_1, s_2)$ in Eq. (10) was calculated in the thread mode, independently for every mesh node. In a similar way, the double integral at the end of expressions (12) was calculated independently at the nodes of meshes created for the integrals over S_3, S_4, and S_5. As a result, one value for the quantity β'_{32} or the sum $\beta'_{44}+\beta'_{45}$ was calculated during about 1 s (at $n = 30$) on the PC with the graphic processor GeForce GTS 450 (instead of 1.5 min). Calculations of one β'_{46}-value at $n = 15$ lasted for about 1 h even if using the GPU.

The table partially exhibits the calculation results obtained for the virial coefficients of the mLJ potential (2), in the dimensionless form $B'_{k+1} = B_{k+1}/\sigma^{3k}$, and for various values of dimensionless temperature $T^* = kT/\epsilon$. The order of integration error magnitude (it was evaluated using Aitken's process [23]) was lower than the order of the last digit in the tabulated values.

In Fig. 4, the dependences of the virial coefficients of various orders on the temperature are shown for both the "primordial" (Eq. (1)) and modified (Eq. (2)) Lennard-Jones potentials. A substantial difference is evident even for the second virial coefficient. In the low-temperature interval, this difference becomes even more appreciable for higher-order coefficients. As the temperature increases, this difference gradually disappears, because the contribution of the most modified potential part, which is responsible for the attraction at large distances, decreases (the repulsion parts of potentials (1) and (2) differ weakly from each other (see Fig. 1)).

In Fig. 5, the dependences $T^*(\rho^*)$, where the $\rho^* = \rho\sigma^3$ is the dimensionless density, are depicted. They correspond to the zero value of isothermal bulk mod-

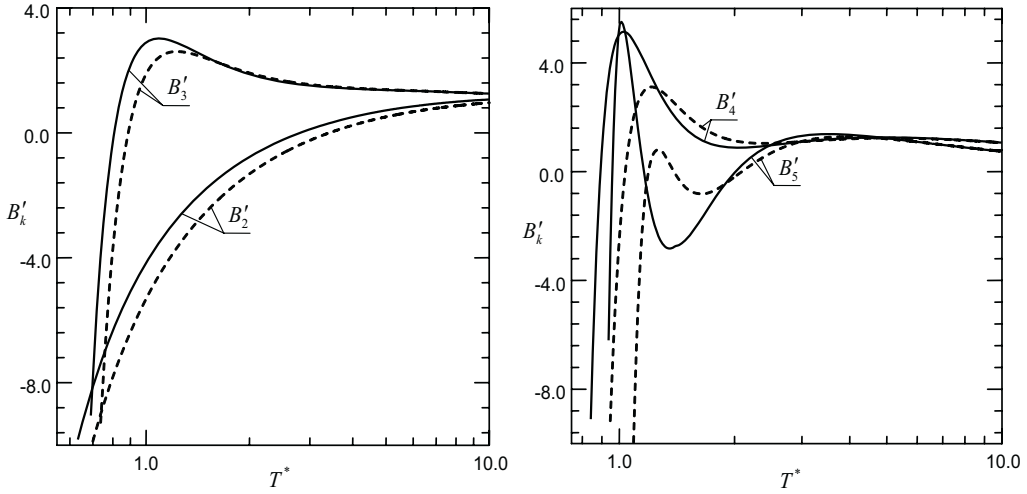

Fig. 4. Temperature dependences of the second and third (left panel) and the fourth and fifth (right panel) virial coefficients for the LJ (dashed curve) and mLJ (solid curve) potentials

ulus (or the singularity of the isothermal compressibility, $(\partial P/\partial V)_T = 0$) and were calculated on the basis of the virial equation of state for mLJ model with the coefficients up to the third, fourth, and fifth orders. Such curves are conventionally associated with spinodals [16, 20], because they confine the thermodynamically forbidden sections of isotherms with negative compressibilities (i.e. absolutely unstable states) described by the virial equation of state. However, the issues concerning the adequacy limits for the virial equation of state itself or whether the equation obtained on the basis of a single-phase statistics developed for infinitely large systems can describe metastable states in general still remain open [24].

Recently, there appeared the researches, whose results testify that just the singularity points of the isothermal compressibility in the virial equation of state are the applicability limits for this equation [25–27], and the very fact that those points belong to the spinodal cannot be considered quite indisputable. Moreover, the behavior of the exact expression for the partition function (in contrast to its virial approximation) at those points corresponds to the beginning of the condensation [25, 26, 28], i.e. to a binodal rather than a spinodal.

At temperatures below the critical one and at low densities (these are states to the left from the experimental binodal in Fig. 5), the virial equation with four or five coefficients produces results that agree well with the experiment (the difference does not exceed 1%). However, as the density grows, the deviation from experimental data increases, and the number of coefficients taken into account in the equation starts to considerably affect the results obtained and the position of curves corresponding to the isothermal compressibility singularity (Fig. 5). It is evident that the higher-order coefficients cannot be neglected in the condensation region (at least, it takes more than five coefficients). In accordance with the results obtained for a different potential in work [28], we may assume that the singularity curve for the isothermal

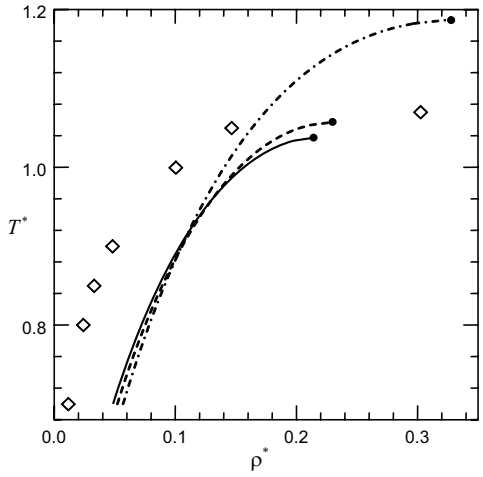

Fig. 5. Curves of the isothermal compressibility singularity calculated for the mLJ system according to the virial equation with three (dash-dotted curve), four (dashed curve), and five (solid curve) coefficients. Symbols (◇) correspond to the experimental binodal [19]

compressibility will be really close to the experimental binodal if higher-order coefficients should be made allowance for.

The values of critical parameters for the mLJ potential obtained with regard for five virial coefficients – namely, $T^* = 1.04$, $\rho^* = 0.22$, and $P^* = P\sigma^3/\epsilon = 0.081$ – turn out somewhat less than the parameters known from numerical experiments – $T^* = 1.07$, $\rho^* = 0.30$,and; $P^* = 0.12$ [19]. This fact may also indicate that the higher-order coefficients should be taken into consideration.

4. Conclusions

The infinite radius of interaction in the Lennard-Jones potential considerably complicates numerical experiments. Therefore, various simplifications of the potential, e.g., the modified Lennard-Jones potential (see Eq. (2)), are used. The same modification is proposed to be applied not only in experimental but also theoretical researches. In this work, the values of the second, third, fourth, and fifth virial coefficients for the modified Lennard-Jones potential in a wide temperature range were obtained. At high temperatures, those coefficients do not differ practically from the coefficients for the primordial Lennard-Jones potential. In the low-temperature interval, on the contrary, the difference becomes very substantial. A comparison of experimental data with the results of numerical simulations testifies that the obtained virial coefficients allow the behavior of the system with the modified Lennard-Jones interaction potential (2) to be described rather well at high densities and supercritical temperatures, as well as at low densities and subcritical temperatures. For the behavior of such a system in the condensation region to be accurately described at the quantitative level, the problem of finding the higher-order virial coefficients still remains challenging.

1. S. Chapman and T.G. Cowling, *The Mathematical Theory of Non-Uniform Gases* (Cambridge Univ. Press, New York, 1970).
2. J. Lennard-Jones, Proc. R. Soc. London, Sect. A **106**, 441 (1924).
3. J. Lennard-Jones, Proc. R. Soc. London, Sect. A **106**, 463 (1924).
4. W.W. Wood and F.R. Parker, J. Chem. Phys. **27**, 720 (1957).
5. L.A. Rowley, D. Nicholson, and N.G. Parsonage, J. Comput. Phys. **17**, 401 (1975).
6. A.Z. Panagiotopoulos, Int. J. Thermophys. **15**, 1057 (1994).
7. X. Feng, Z. Li, and Z. Guo, Chin. Sci. Bull. **45**, 2004 (2000).
8. D.A. Kofke, J. Chem. Phys. **98**, 4149 (1993).
9. D. Frenkel and B. Smit, *Understanding Molecular Simulation: From Algorithms to Applications* (Academic Press, San Diego, CA, 2002).
10. J.K. Johnson, J.A. Zollweg, and K.E. Gubbins, Mol. Phys. **78**, 591 (1993).
11. P. Attard, J. Chem. Phys. **116**, 9616 (2002).
12. J. Nicolas, K. Gubbins, W. Streett, and D. Tildesley, Mol. Phys. **37**, 1429 (1979).
13. A. Lotfi, J. Vrabec, and J. Fischer, Mol. Phys. **76**, 1319 (1992).
14. W.-Z. Ou-Yang, Z.-Y. Lu, T.-F. Shi, Z.-Y. Sun, and L.-J. An, J. Chem. Phys. **123**, 234502 (2005).
15. B. Smit, J. Chem. Phys. **96**, 8639 (1992).
16. K.R.S. Shaul, A.J. Schultz, and D.A. Kofke, Coll. Czech. Chem. Commun. **75**, 447 (2010).
17. J.Q. Broughton and G.H. Gilmer, J. Chem. Phys. **79**, 5095 (1983).
18. T. Sakagami and K. Fuchizaki, J. Phys.: Conf. Ser. **215**, 012123 (2010).
19. Y. Asano and K. Fuchizaki, J. Chem. Phys. **137**, 174502 (2012).
20. A.J. Schultz and D.A. Kofke, Mol. Phys. **107**, 2309 (2009).
21. A.J. Schultz, N.S. Barlow, V. Chaudhary, and D.A. Kofke, Mol. Phys. **111**, 535 (2013).
22. J.E. Mayer and M.G. Mayer, *Statistical Mechanics* (Wiley, New York, 1977).
23. V.I. Krylov, *Approximate Calculation of Integrals* (Dover, Mineola, NY, 2006).
24. G.A. Martynov, Physics-Uspekhi **42**, 517 (1999).
25. M.V. Ushcats, Visn Kharkiv. Nats. Univ. **1020**, 6 (2012).
26. M.V. Ushcats, Phys. Rev. Lett. **109**, 040601 (2012).
27. M.V. Ushcats, Phys. Rev. E **87**, 042111 (2013).
28. M.V. Ushcats, J. Chem. Phys. **138**, 094309 (2013).

Received 10.06.13.
Translated from Ukrainian by O.I. Voitenko

М.В. Ушкац

ВІРІАЛЬНІ КОЕФІЦІЄНТИ ДЛЯ МОДИФІКОВАНОГО ПОТЕНЦІАЛУ ЛЕНАРД-ДЖОНСА

Р е з ю м е

Розглянуто модифікований потенціал Ленард-Джонса, який має кінцевий радіус взаємодії і значно спрощує числове моделювання термодинамічних систем великої густини, зберігаючи, при цьому, його реалістичність. Для цього потенціалу розраховані віріальні коефіцієнти до п'ятого порядку, включно, в широкому діапазоні температур, що дозволяє використовувати потенціал не лише в числових експериментах, а і в теоретичних дослідженнях. запропоновано використання цього потенціалу в ролі еталона для оцінки адекватності різних теоретичних і експериментальних підходів.